

# Emission engineering in germanium nanoresonators

*Michele Celebrano<sup>1</sup>, Milena Baselli<sup>1</sup>, Monica Bollani<sup>2</sup>, Jacopo Frigerio<sup>3</sup>, Andrea Bahgat Shehata<sup>4</sup>, Adriano Della Frera<sup>4</sup>, Alberto Tosi<sup>4</sup>, Andrea Farina<sup>5</sup>, Fabio Pezzoli<sup>6</sup>, Johann Osmond<sup>7</sup>, Xiaofei Wu<sup>8</sup>, Bert Hecht<sup>8</sup>, Roman Sordan<sup>3</sup>, Daniel Chrastina<sup>3</sup>, Giovanni Isella<sup>3</sup>, Lamberto Duò<sup>1</sup>, Marco Finazzi<sup>1</sup>, Paolo Biagioni<sup>1,\*</sup>*

<sup>1</sup> *Dipartimento di Fisica and LNESS, Politecnico di Milano, piazza Leonardo da Vinci 32, 20133 Milano, Italy.*

<sup>2</sup> *Consiglio Nazionale delle Ricerche, Istituto di Fotonica e Nanotecnologie, via Anzani 42, 22100 Como, Italy.*

<sup>3</sup> *CNISM and LNESS, Dipartimento di Fisica del Politecnico di Milano, Polo Regionale di Como, via Anzani 42, 22100 Como, Italy.*

<sup>4</sup> *Dipartimento di Elettronica, Informazione e Bioingegneria, Politecnico di Milano, piazza Leonardo da Vinci 32, 20133 Milano, Italy.*

<sup>5</sup> *Consiglio Nazionale delle Ricerche, Istituto di Fotonica e Nanotecnologie, piazza Leonardo da Vinci 32, 20133 Milano, Italy.*

<sup>6</sup> *LNESS-Dipartimento di Scienza dei Materiali, Università degli Studi di Milano-Bicocca, via R. Cozzi 55, 20125 Milano, Italy.*

<sup>7</sup> *ICFO-Institut de Ciències Fotoniques, Av. Carl Friedrich Gauss, 3, 08860 Castelldefels, Barcelona, Spain.*

<sup>8</sup> *Nano-Optics & Biophotonics Group, Department of Experimental Physics 5, Röntgen Research Center for Complex Materials (RCCM), Physics Institute, University of Würzburg, Am Hubland,*

97074 Würzburg, Germany.

\* to whom correspondence should be addressed: paolo.biagioni@polimi.it

KEYWORDS. Silicon photonics, germanium emitter, optical antennas, Fabry-Pérot cavity resonators

## ABSTRACT

We experimentally investigate the smallest germanium Fabry-Pérot cavity resonators on silicon that can be designed to work around 1.55  $\mu\text{m}$  wavelength and observe an almost 30-fold enhancement in the collected spontaneous emission per unit volume when compared to a continuous germanium film of the same thickness. The enhancement is due to an effective combination of (i) excitation enhancement at the pump wavelength, (ii) emission enhancement (Purcell effect) at the emission wavelength, and (iii) effective beaming by the nanoresonators, acting as optical antennas to enhance the radiation efficiency. Our results set a basis for the understanding and engineering of emitting devices based on subwavelength, CMOS-compatible nanostructures operating at telecommunication wavelengths.

## TEXT

Over the last decade germanium has been proposed as one of the most promising materials for light detection, modulation, and emission in silicon-photonics architectures [1-3]. Its direct band-gap, which is only about 140 meV larger than the fundamental indirect band-gap, ensures excellent absorption and promising emission properties, which recently led to the realization of integrated photodetectors [4-7], electroluminescent devices [8,9], and to the demonstration of optically-pumped [10] and electrically-pumped [11] Ge lasers. An attractive feature of the Ge optical properties is the matching between the direct emission band and the conventional

telecommunication window around the 1.55  $\mu\text{m}$  wavelength. Along the road towards integrated Ge light sources, significant efforts have been devoted to material engineering in terms of strain [12-16] and doping [10,17], in order to make radiative recombination more effective and to create the conditions for population inversion and gain [18,19]. Also photonic engineering has been applied, although to a lesser extent, in order to establish cavity resonances at the desired emission wavelengths. A particularly appealing perspective, leading to compact and cost-effective solutions, is the direct shaping of the active Ge material as a cavity for photons, which allows one to spectrally purify, enhance, and re-direct photon emission. While this concept has been successfully applied to the development of waveguide [20,21], photonic-crystal [22], and disk resonators [23], the overall size of these photonic devices was generally much larger (from several  $\mu\text{m}$  to mm size) than the free-space operating wavelength  $\lambda_0$ , although, in principle, the volume of a resonant dielectric cavity can be as small as about  $(\lambda_0/2n)^3$ ,  $n$  being the refractive index of the dielectric. It is one of the main paradigms of nano-optics that size reduction of modal volumes can increase light-matter interaction and boost the Purcell factor for light emission, thus possibly reducing the threshold for lasing. Moreover, the trend towards smaller light sources is clearly driven by the perspective integration of nano-devices with largely reduced footprints.

In this work we design, fabricate, and experimentally characterize Ge nanoresonators on Si in the form of truncated waveguides with a fixed section profile of about  $400 \times 400 \text{ nm}^2$ , i.e. very close to the cut-off conditions for the waveguide, and with a length  $L$  varying from 500 nm to 1400 nm. We characterize their Fabry-Pérot resonances by scanning confocal photoluminescence microscopy and observe on resonance a 27-fold enhancement in the collected emission per unit volume when compared with a continuous Ge film having the same thickness.

The investigated nanostructures were fabricated by focused ion-beam (FIB) milling starting from a 400-nm-thick Ge film heavily-doped with phosphorous (activated dopant density  $N_D \sim 1-2 \times 10^{19} \text{ cm}^{-3}$ ), grown on Si(001) wafers by low-energy plasma-enhanced chemical vapor deposition [24]. After the growth process, the sample was subjected to a series of annealing cycles between 600 and 780°C to reduce the density of dislocations threading from the interface to the sample surface. Due to the difference between the thermal expansion coefficient of Ge and Si [25,26] the Ge film acquires a tensile strain of approximately  $0.22 \pm 0.01\%$ , as quantified by means of x-ray diffraction (see Supporting Information). The surface is then covered by a thermally-evaporated silicon oxide film with a thickness of about 50 nm. Such a protective layer is extremely effective in improving the quality of FIB milling (see Supporting Information) and being transparent in the wavelength range considered here it has no significant effects on the optical properties of the nanoresonators. The FIB patterning of the Ge epitaxial layers likely induces a modification of the thermally-induced strain, since lateral dimensions become comparable with the film thickness. The original bi-axial stress evolves towards a position-dependent tri-axial stress [27] and the formation of free surfaces is expected to allow, on average, elastic relaxation of the initial stress. A representative scanning electron microscopy (SEM) image of a resulting nanoresonator is shown in Fig. 1(a), where the protective  $\text{SiO}_x$  layer and the slightly tilted wall geometry are also visible.

The fabricated structures can be treated as finite pieces of waveguides, whose end facets act as cavity mirrors. Fabry-Pérot resonances in such resonators originate from the self-interference of guided modes bouncing back and forth in the truncated waveguide. As a result, the local density of optical states available for the radiative decay of excited electron-hole pairs is suppressed off resonance and enhanced on resonance. In the latter case, the rate of spontaneous emission is

therefore increased, an effect known as the Purcell effect, which was originally invoked to describe lossless cavities but can be extended to lossy materials as well [28]. For a given guided mode with effective wavelength  $\lambda_{\text{eff}}$ , Fabry-Pérot resonances occur at waveguide lengths  $L_{\text{res}} = m \frac{\lambda_{\text{eff}}}{2}$ , where  $m$  is an integer defining the resonance order. We compute the spatial field distribution associated to each waveguide mode by means of the finite-difference frequency-domain (FDFD) method [29]. While for sections larger than about  $400 \times 400 \text{ nm}^2$  higher-order modes start to appear, for smaller sections cut-off conditions are gradually approached, with the guided modes being less and less confined inside the Ge waveguide (see Supporting Information). We find that, for a model waveguide made of the above-described material with a section of about  $400 \times 400 \text{ nm}^2$  and a free-space wavelength  $\lambda_0 \cong 1550 \text{ nm}$ , only the two almost-degenerate lowest-order quasi-TE and quasi-TM modes are present [Fig. 1(b) and Fig. 1(c), respectively], being characterized by a dominant electric field oriented parallel and perpendicular to the substrate plane, respectively. The calculated index of these almost degenerate modes, for a geometry closely resembling the fabricated one, is  $n \cong 3.6 + i0.01$  and their effective wavelength is therefore  $\lambda_{\text{eff}} \cong 430 \text{ nm}$ .

We recorded spatial maps collecting the direct-gap Ge spontaneous emission at room temperature by means of scanning confocal microscopy, employing a standard long-working-distance achromatic objective (N.A. = 0.7) and an excitation diode laser emitting at 980 nm wavelength (see Supporting Information), providing an experimental lateral resolution of about  $1.3 \mu\text{m}$ . The average power impinging on the objective is kept in a range between 1 and 10 mW, corresponding to a power density of about  $10^4$ - $10^5 \text{ W/cm}^2$ . The different spectral components of the collected emission are separated inside a Pellin Broca prism [30] and then focused onto a InGaAs/InP single-photon avalanche diode (SPAD) [31], whose active area ( $25 \mu\text{m}$  diameter)

acts as a spatial filter in the image plane for wavelength selection and background rejection. The spectral resolution is about 15 nm in the spectral range of interest.

Representative room-temperature luminescence maps of each individual nanoresonator obtained by selecting a spectral window around 1550 nm are shown in the bottom part of Fig. 2, together with the respective SEM images. While for shorter resonators the confocal images show a single lobe as the result of the convolution between the nanostructure and the illumination Gaussian beam, cavities whose length is comparable with (or larger than) the lateral resolution of the microscope show a double-lobe image, because of the enhanced scattered emission at the end of the resonator [21]. A quantitative analysis of the measured enhancement is performed by extracting the emission per unit volume from the experimental map of each nanocavity and normalizing it to that of a continuous Ge film with the same thickness (unprocessed region of the same sample), taking the dimensions of the focal spot and the size of each nanostructure into account (see Supporting Information). The results are shown in the top part of Fig. 2 as a function of the nanoresonator length. They demonstrate an up to 27-fold enhancement in the collected emission intensity from the resonators compared to the film. A striking feature is the presence of maxima in the experimental emission enhancement for lengths roughly around 600, 850, 1100, and 1300 nm, i.e. with a length periodicity of about 235 nm. This value is in close coincidence to the periodicity of  $\frac{\lambda_{\text{eff}}}{2} \cong 215$  nm expected for Fabry-Pérot oscillations, as estimated from the FDFD simulations discussed above.

We perform a three-step analysis of the investigated sample geometry using finite-difference time-domain (FDTD) simulations [32] in order to disentangle the different contributions to the observed overall enhancement [Fig. 3(a), see Supporting Information for details on the

simulations]. This approach considers (i) the enhancement in the absorbed power per unit volume by the resonator after 980-nm Gaussian beam illumination (red solid line, circles); (ii) the enhancement in the total emitted power at 1550 nm by a set of uncorrelated dipoles uniformly distributed inside the resonator to mimic spontaneous emission (blue line, triangles), and (iii) the enhancement due to changes in the emission directionality and radiation efficiency related to the fraction of emitted power falling within the objective's collection angle in the air half space (black line, squares). Regarding the first contribution, it should be noted that no resonances are observed, as expected because of the large losses in the material at the pump wavelength. However, confined structures can non-resonantly absorb a larger fraction of power per unit volume than continuous films, for a fixed excitation fluency, because of the light-trapping contribution coming from high-index-contrast boundary conditions. The second contribution is calculated as the ratio of total emitted power by the dipoles inside the resonator and inside the continuous film. It should be noted that, in order to simulate uncorrelated dipoles and avoid spurious interference effects,  $N$  individual simulations need to be run to consider a set of  $N$  dipoles, one for each dipole. The third contribution is computed by projecting the local dipole fields to the far field and calculating the flux of the Poynting vector within the objective's collection angle. By combining the results of the three analysis steps, we are able to quantify the overall enhancement in the collected emission, as shown in Fig. 3(b) (black line, circles). This is in very nice quantitative agreement with the experimental results (also shown in the same panel for comparison, red line, squares). The residual deviation between experimental and simulation results for the shorter nanoresonators may be due to a larger degree of elastic strain relaxation (and therefore lower efficiency for radiative recombination) as the length of the resonator is reduced [33].

Noticeably, most of the enhancement is related to the third contribution, i.e. to the enhanced radiation of the light emitted by the nanoresonators within the objective collection angle (antenna effect) [34]. To gain a better understanding of the phenomenon, we plot in Fig. 4 the emission angular pattern in the upper air half-space and in the lower Si half-space for a resonant structure (a) and for the continuous film (b). The same set of uncorrelated dipoles mentioned above is also used for these calculations. It can be seen that two effects take place in the nanoresonators compared to the continuous film: (i) an increase in the fraction of emitted photons that are beamed towards the air half-space compared to those that are emitted towards the substrate, with the nanoresonator beaming a larger fraction of the radiated photons towards the air half-space, and (ii) a drastic difference in the total number of radiated photons (note the different intensity scales for the two plots). The analysis shows that this drastic enhancement in the radiation efficiency is not related to a larger emission rate for the dipoles in the nanoresonator compared to the film, rather it is due to the large fraction of light that is waveguided and trapped inside the continuous film, which adds a further non-radiative loss channel for the film. The enhancement in the total emitted power (second step of the simulation analysis described above) is indeed particularly low due to the small quality factor of the resonances, mainly caused by the low reflectivity of the waveguide facets that is estimated to be around 68 % (see Supporting Information). Nevertheless, Fabry-Pérot contributions are unambiguously detected as periodic oscillations in the emission signal as a function of the cavity length. In perspective, the quality factor of the Fabry-Pérot resonances could be improved by fabricating steeper end facets or by a more advanced level of nanophotonic engineering, which would include for example nanostructured Bragg mirrors.

Fabry-Pérot cavity resonances are also expected to have an effect on the spectral shape of the emission band, by enhancing those wavelength components that are on resonance with the cavity and suppressing those that are off resonance. Indeed, Fig. 5(a) shows the periodic modulation of the emission spectrum measured on resonators of varying length and therefore varying resonant wavelength. The steep drop around 1600 nm represents the cut-off of the InGaAs/InP SPAD (see Supporting Information) and does not allow for a quantitative analysis of the resulting spectral shape.

It should be noted that we observed no experimental dependence of the emitted intensity on the linear polarization direction of the excitation beam. This should be expected because of the incoherent processes at the basis of spontaneous emission (where no memory is kept of the excitation polarization), which implies that the probability for an excited electron-hole pair to decay into a mode of the cavity with specific polarization properties is independent of the polarization of the excitation beam. Also, we found no net polarization of the emitted photons, meaning that the ratio  $R = \frac{I_{\perp}}{I_{\parallel}}$  between the emitted light intensity polarized perpendicular and parallel to the resonator axis is always around 1, with deviations below 20% among different samples. While this would not be expected for an emission process mediated by a Fabry-Pérot cavity, it should be recalled that the two almost degenerate quasi-TE and quasi-TM modes possess very different polarization properties. When this is taken into account and the far field polarization for the ensemble of uncorrelated emitters is simulated, we find that only a residual  $R \cong 2.5$  would be expected on average (see Supporting Information). We tentatively attribute the additional depolarization to residual wall roughness, which depolarizes the photons emitted by the Ge nanocavities. Finally, we experimentally observed a proportionality between the excitation power and the emission rate from the nanoresonators, as shown in Fig. 5(b), therefore

finding no evidence of background due to thermal blackbody emission [35] and also ruling out any stimulated emission for the investigated excitation rates.

In conclusion, we studied the smallest possible waveguide Fabry-Pérot resonators that can be realized with Ge on Si and demonstrated an almost 30-fold enhancement in the collected emission per unit volume at 1.55  $\mu\text{m}$  wavelength, when compared to that from a continuous film with the same thickness. Detailed simulations reveal that most of the enhancement is due to effective beaming of the emitted photons within the collection angle of the objective, demonstrating that the nanostructures act as efficient directional antennas to improve the radiation efficiency and confirming the key importance of a thorough analysis of emission enhancement processes from confined nanostructures to unambiguously assess their physical origin. In perspective, the performance of the resonators can be improved by strain engineering to further enhance the emission efficiency or by nano-photonic engineering of the cavity mirrors (e.g. fabricating steeper facets and/or Bragg reflectors) to enhance the quality factor of the resonances. The analysis and experimental results presented in this work therefore pave the road towards optimized group-IV nanoemitters where doping, strain, and photonic engineering can be merged together to achieve highly directional and efficient light emission at telecommunication wavelengths.

## FIGURES

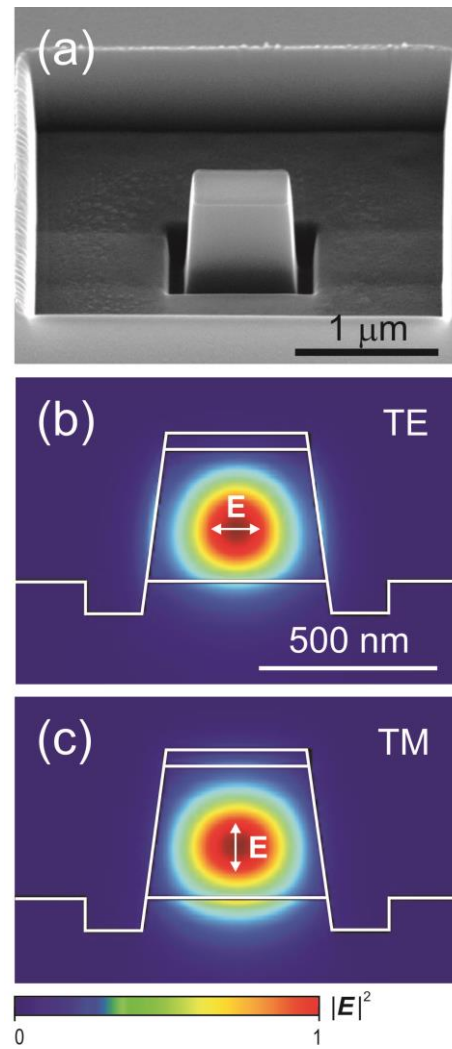


**Figure 1.** (a) SEM image of a Ge nanoresonator. The thin oxide protective layer and the slightly tilted lateral walls, due to the FIB beam profile, are also visible. (b) Field intensity map of the lowest-order (b) quasi-TE and (c) quasi-TM mode in the Ge waveguide, calculated by FDFD on a model structure closely resembling the nanoresonators under study.

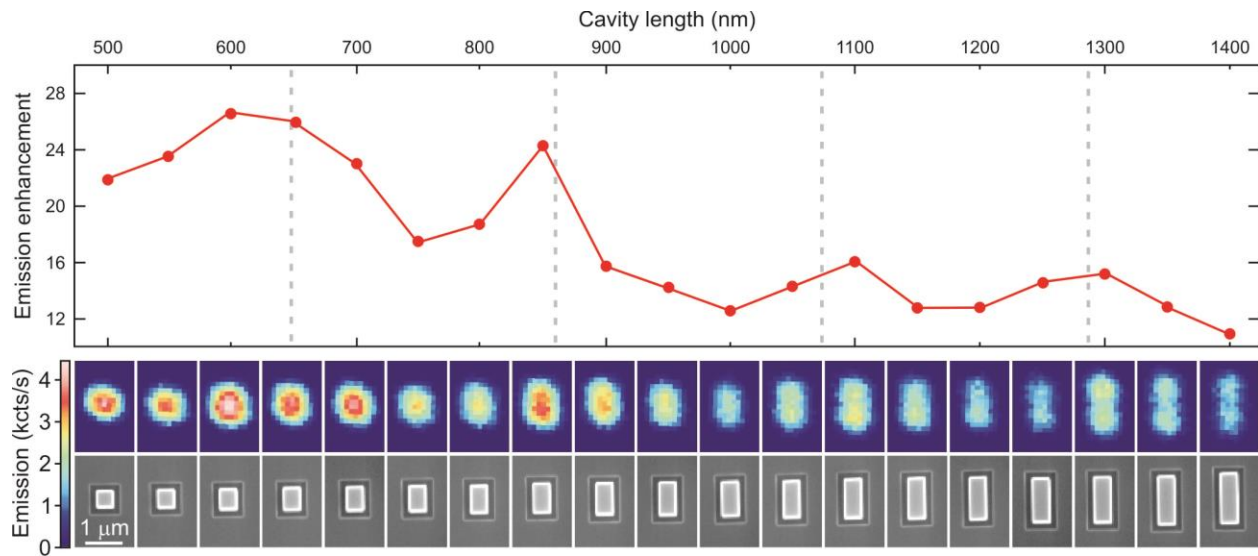


**Figure 2.** Lower panel: SEM and room-temperature confocal luminescence maps of the array of nanoresonators with length varying between about 500 nm and 1400 nm in steps of 50 nm. Upper panel: Experimental enhancement in the collected emission per unit volume from each individual Ge nanoresonator, normalized to the emission from a continuous Ge film of the same thickness. Each data point is the result of averaging over three different samples fabricated from the same Ge substrate with the same nominal dimensions. Dashed vertical lines represent the spectral position of Fabry-Pérot resonances expected on the basis of FDFD and FDTD simulations.

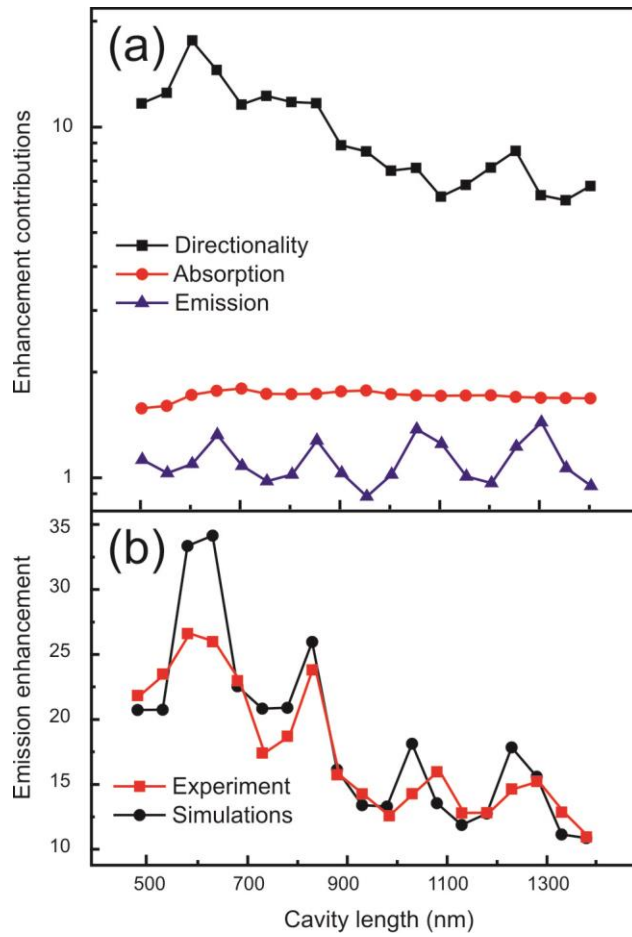


**Figure 3.** (a) Individual contributions to the total enhancement obtained from simulation results: increase in the absorbed power per unit volume (red line, circles), emission enhancement (blue line, triangles), and directional emission (black line, squares). (b) Results of FDTD simulations for the total enhancement per unit volume (black line, circles) and their quantitative comparison with the experimental results (red line, squares).

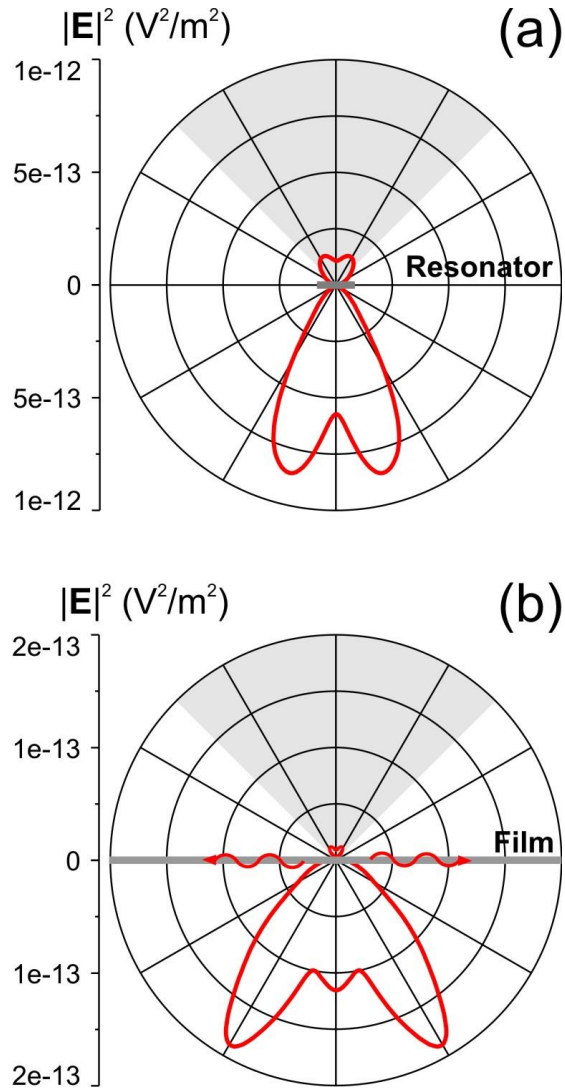


**Figure 4.** Angular distribution of the electric field intensity after far-field projection onto a sphere of 1 m radius, both for the upper air half-space and the lower Si half-space, for a set of uncorrelated dipoles emitting a total power of 1 W in vacuum: (a) nanoresonator ( $L = 600$  nm), (b) continuous Ge film of the same thickness. The angular patterns are plotted on a plane perpendicular to the resonator main axis. The grey cone represents the collection angle of the objective in the air half-space, while the wavy arrows represent non-radiative losses related to waveguided light trapping inside the Ge film. Note the different intensity scales for the two panels.

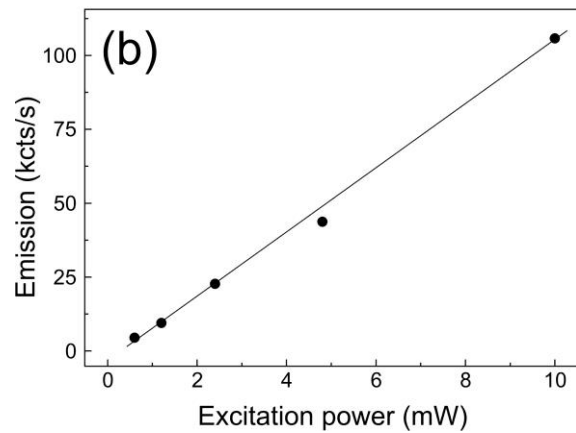
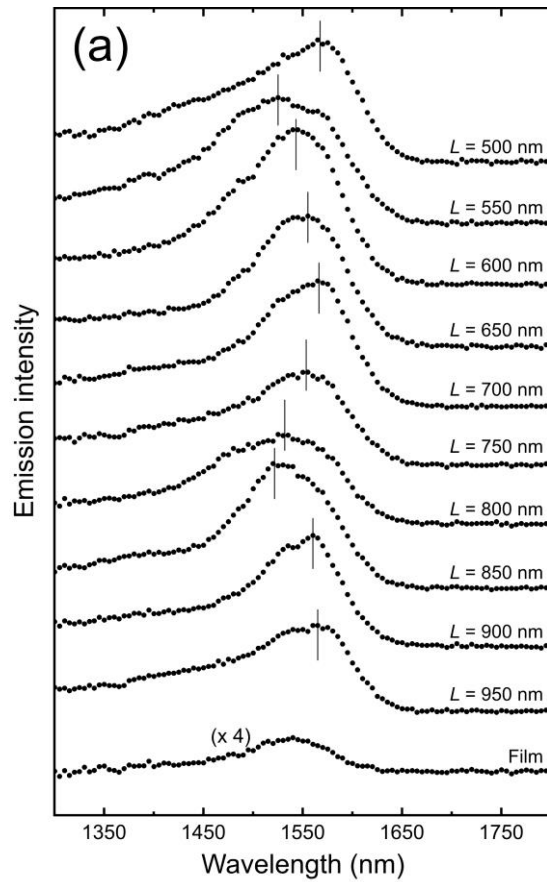


**Figure 5.** (a) Experimental room-temperature photoluminescence spectra from individual Ge nanoresonators and from the reference continuous Ge film, acquired with the same excitation power. (b) Representative emission rate from a resonant cavity as a function of the excitation power.

## ACKNOWLEDGMENTS

The authors would like to thank Jord C. Prangma for insightful discussions on emission enhancement in lossy media. Funding from Fondazione Cariplo under the project “Nano antennas of germanium for advanced photonics (NANOGAP)” (project number 2010-0632) and from Regione Lombardia through the grant “Dote ricercatori” are gratefully acknowledged.

## REFERENCES

- [1] Soref, R. *Silicon* **2010**, 2, 1.
- [2] Liang, D.; Bowers, J. E. *Nat. Photonics* **2010**, 4, 511.
- [3] Boucaud, P.; El Kurdi, M.; Ghrib, A.; Prost, M.; de Kersauson, M.; Sauvage, S.; Aniel, F.; Checoury, X.; Beaudoin, G.; Largeau, L.; Sagnes, I.; Ndong, G.; Chaigneau, M.; Ossikovski, R. *Photon. Res.* **2013**, 1, 102.
- [4] Osmond, J.; Isella, G.; Chrastina, D.; Kaufmann, R.; Acciarri, M.; von Känel, H. *Appl. Phys. Lett.* **2009**, 94, 201106.
- [5] Cao, L.; Park, J.-S.; Fan, P.; Clemens, B.; Brongersma, M. L. *Nano Lett.* **2010**, 10, 1229.
- [6] Kaufmann, R.; Isella, G.; Sanchez-Amores, A.; Neukom, S.; Neels, A.; Neumann, L.; Brenzikofer, A.; Dommann, A.; Urban, C.; von Känel, H. *J. Appl. Phys.* **2011**, 110, 023107.
- [7] Vivien, L.; Polzer, A.; Marris-Morini, D.; Osmond, J.; Hartmann, J. M.; Crozat, P.; Cassan, E.; Kopp, Ch.; Zimmermann, H.; Fédéli, J. M. *Opt. Exp.* **2012**, 20, 1096.
- [8] Sun, X.; Liu, J.; Kimerling, L. C.; Michel, J. *Opt. Lett.* **2009**, 34, 1198.

- [9] de Kersauson, M.; Jakomin, R.; El Kurdi, M.; Beaudoin, G.; Zerounian, N.; Aniel, F.; Sauvage, S.; Sagnes, I.; Boucaud, P. *J. Appl. Phys.* **2010**, 108, 023105.
- [10] Liu, J.; Sun, X.; Pan, D.; Wang, X.; Kimerling, X. W.; Koch, Th. L.; Michel, J. *Opt. Exp.* **2007**, 15, 11272.
- [11] Camacho-Aguilera, R. E.; Cai, Y.; Patel, N.; Bessette, J. T.; Romagnoli, M.; Kimerling, L. C.; Michel, J. *Opt. Exp.* **2012**, 20, 11316.
- [12] El Kurdi, M.; Bertin, H.; Martincic, E.; de Kersauson, M.; Fishman, G.; Sauvage, S.; Bosseboeuf, A.; Boucaud, P. *Appl. Phys. Lett.* **2010**, 96, 041909.
- [13] Huo, Y.; Lin, H.; Chen, R.; Makarova, M.; Rong, Y.; Li, M.; Kamins, Th. I.; Vuckovic, J.; Harris, J. S. *Appl. Phys. Lett.* **2011**, 98, 011111.
- [14] Sánchez-Pérez, J. R.; Boztug, C.; Chen, F.; Sudradjat, F. F.; Paskiewicz, D. M.; Jacobson, R. B.; Lagally, M. G.; Paiella, R. *Proc. Natl. Acad. Sci.* **2011**, 108, 18893.
- [15] Jain, J. R.; Hryciw, A.; Baer, Th. M.; Miller, D. A. B.; Brongersma, M. L.; Howe, R. T. *Nat. Photonics* **2012**, 6, 398.
- [16] Süess, M. J.; Geiger, R.; Minamisawa, R. A.; Schiefler, G.; Frigerio, J.; Chrastina, D.; Isella, G.; Spolenak, R.; Faist, J.; Sigg, H. *Nat. Photonics* **2013**, 7, 466.
- [17] El Kurdi, M.; Kociniewski, T.; Ngo, T.-P.; Boulmer, J.; Débarre, D.; Boucaud, P.; Damlencourt, J. F.; Kermarrec, O.; Bensahel, D. *Appl. Phys. Lett.* **2009**, 94, 191107.
- [18] Carroll, L.; Friedli, P.; Neuenschwander, S.; Sigg, H.; Cecchi, S.; Isa, F.; Chrastina, D.; Isella, G.; Fedoryshyn, Y.; Faist, J. *Phys. Rev. Lett.* **2012**, 109, 057402.

- [19] Dutt, B.; Sukhdeo, D. S.; Nam, D.; Vulovic, B. M.; Yuan, S.; Saraswat, K. C. *IEEE Photon. J.* **2013**, 4, 2002.
- [20] Liu, J.; Sun, X.; Camacho-Aguilera, R.; Kimerling, L. C.; Michel, J. *Opt. Lett.* **2010**, 35, 679.
- [21] de Kersauson, M.; El Kurdi, M.; David, S.; Checoury, X.; Fishman, G.; Sauvage, S.; Jakomin, R.; Beaudoin, G.; Sagnes, I.; Boucaud, P. *Opt. Exp.* **2011**, 19, 17925.
- [22] Boucaud, P.; El Kurdi, M.; David, S.; Checoury, X.; Li, X.; Ngo, T.-P.; Sauvage, S.; Bouchier, D.; Fishman, G.; Kermarrec, O.; Campidelli, Y.; Bensahel, D.; Akatsu, T.; Richtarch, C.; Ghyselen, B. *Thin Solid Films* **2008**, 517, 121.
- [23] Shambat, G.; Cheng, S.-L.; Lu, J.; Nishi, Y.; Vuckovic, J. *Appl. Phys. Lett.* **2010**, 97, 241102.
- [24] Rosenblad, C.; Deller, H. R.; Dommann, A.; Meyer, T.; Schroeter, P.; von Känel, H. *J. Vac. Sci. Technol. A* **1998**, 16, 2785.
- [25] Slack, G. A.; Bartram, S. F. *J. Appl. Phys.* 1975, 46, 89.
- [26] Capellini, G.; De Seta, M.; Zaumseil, P.; Kozlowski, G.; Schroeder, T. *J. Appl. Phys.* **2012**, 111, 073518.
- [27] Jain, S. C.; Harker, A. H.; Atkinson, A.; Pinardi, K. J. *Appl. Phys.* **1995**, 78, 1630.
- [28] Sauvan, C.; Hugonin, J. P.; Maksymov, I. S.; Lalanne, P. *Phys. Rev. Lett.* **2013**, 110, 237401.

- [29] MODE Solutions, version 6.0.3, Lumerical Solutions, Inc., Canada.
- [30] Bargigia, I.; Tosi, A.; Bahgat Shehata, A.; Della Frera, A.; Farina, A.; Bassi, A.; Taroni, P.; Dalla Mora, A.; Zappa, F.; Cubeddu, R.; Pifferi, A. *Appl. Spectr.* **2012**, 66, 944.
- [31] Tosi, A.; Della Frera, A.; Bahgat Shehata, A.; Scarcella, C. *Rev. Sci. Instrum.* 2012, 83, 013104.
- [32] FDTD Solutions, version 8.5.3, Lumerical Solutions, Inc., Canada.
- [33] Chrastina, D.; Vanacore, G. M.; Bollani, M.; Boye, P.; Schöder, S.; Burghammer, M.; Sordan, R.; Isella, G.; Zani, M.; Tagliaferri, A. *Nanotechnology* **2012**, 23, 155702.
- [34] Biagioni, P.; Huang, J.-S.; Hecht, B. *Rep. Prog. Phys.* **2012**, 75, 024402.
- [35] Boucaud, P.; El Kurdi, M.; Sauvage, S.; de Kersauson, M.; Ghrib, A.; Checoury, X. *Nat. Photonics*, **2013**, 7, 162.